ISSN 1063-7761, Journal of Experimental and Theoretical Physics, 2015, Vol. 120, No. 4, pp. 725–732. © Pleiades Publishing, Inc., 2015.
Original Russian Text © S.V. Yablonskii, V.V. Bondarchuk, E.A. Soto-Bustamante, P.N. Romero-Hasler, M. Ozaki, K. Yoshino, 2015, published in Zhurnal Eksperimental'noi i Teoreticheskoi Fiziki, 2015, Vol. 147, No. 4, pp. 837–845.

STATISTICAL, NONLINEAR, AND SOFT MATTER PHYSICS

Longitudinal and Transverse Pyroelectric Effects in a Chiral Ferroelectric Liquid Crystal

S. V. Yablonskii[a,e], V. V. Bondarchuk[a], E. A. Soto-Bustamante[b], P. N. Romero-Hasler[b], M. Ozaki[c], and K. Yoshino[d]

[a] *Shubnikov Institute of Crystallography, Russian Academy of Sciences, Moscow, 119333 Russia*
[b] *Universidad de Chile, Santiago, 1058 Chile*
[c] *Department of Electronic Engineering, Faculty of Engineering, Osaka University, 2-1 Yamata-Oka, Suita, Osaka, 565-0871 Japan*
[d] *Shimane Institute for Industrial Technology, Matsue, Japan*
[e] *Landau Institute for Theoretical Physics, Russian Academy of Sciences, Chernogolovka, Moscow oblast, 142432 Russia*
e-mail: yablonskii2005@yandex.ru

Received September 16, 2014

Abstract—In this study, we compare the results of experimental investigations of longitudinal and transverse pyroelectric effects in a chiral ferroelectric crystal. In a transverse geometry, we studied freely suspended liquid-crystal films. In both geometries, samples exhibited bistability, demonstrating stable pyroelectric signals of different polarities at zero voltage. It is shown that a bistable cell based on a freely suspended film requires 40 times less energy expenditures as compared to the conventional sandwich-type cell.

DOI: 10.1134/S1063776115040172

1. INTRODUCTION

The pyroelectric effect is one of the oldest known physical effects [1]. The pyroelectric effect is observed in crystals (or textures) belonging to one of ten polar crystallographic point symmetry groups or three limiting groups. The limiting symmetry groups include the symmetry groups of static and rotating (right and left) cones. The symmetry conditions for observation of the pyroelectric effect are necessary but not sufficient conditions. For example, the pyroelectric effect is practically impossible in solids with a high electrical conductivity (e.g., in substances with metal-type conductivity even if they have a polar symmetry group). The detection of the pyroelectric effect can be problematic for $P_s(T) \approx$ const in a certain temperature interval, where $P_s(T)$ is the spontaneous polarization as a function of temperature. It is well known that the pyroelectric effect has a much lower sensitivity and detectivity as compared to effects based on the generation of electron–hole pairs. For instance, the current sensitivity of a silicon-based photodetector in the visible range is usually about 1 A/W and its detectivity $D^* = 1 \times 10^{13}$ cm $Hz^{1/2}$ W^{-1} ($\lambda = 1$ μm, $T = 300$ K). At the same time, the maximal current sensitivity for lanthanum-modified lead zirconate titanate (PZT), which is one of the best pyroelectrics, does not exceed 50 μA/W, and the maximal detectivity is 6.4×10^8 cm $Hz^{1/2}$ W^{-1} [1]. However, pyroelectric detectors have a considerable advantage over photodetectors. The main merit of pyroelectric detectors is a wide spectral interval of sensitivity. The spectral sensitivity per unit incident power in pyroelectric detectors depends only on the radiant emittance of the detecting surface, which can be close to the blackbody emittance (i.e., close to unity in a wide spectral interval from the visible to the far infrared ranges) [2, 3]. In addition, the pyroelectric signal is proportional to the rate of temperature variation, which can be higher than the space charge relaxation rate. Thus, detectors based on the pyroelectric effect can detect optical signals in the spectral range inaccessible to contemporary photodetectors. The speed characteristics of pyroelectric detectors are also worth noting because such detectors can record rapid processes with a duration on the order of 100 ps [4].

Pyroelectric detectors are mainly used in the so-called longitudinal geometry, in which the Poynting vector of the electromagnetic energy being detected is parallel to the spontaneous polarization and perpendicular to the detector electrodes. In this geometry, the pyroelectric effect exhibits the highest voltage–power sensitivity as compared to the transverse geometry, in which the power flux being detected is perpendicular to the spontaneous polarization [4]. Applications of pyroelectrics for detecting pulsed gamma-radiation are also of interest [5]. As a rule, the detection of a short pulse requires a low capacitance of the sensitive element, which is difficult to obtain using thin films. The transverse geometry is preferable exactly for detecting pulsed radiation, because a pickup with a low capacitance and a large aperture can be obtained in this geometry.

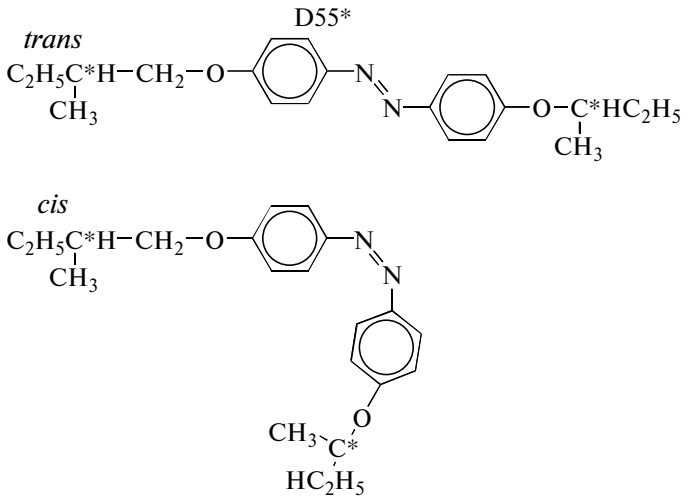

Fig. 1. Chemical formula of D55* mesogenic chiral azo dye. Geometrical trans- and cis-isomers of azo dye are shown.

It should also be noted that although the pyroelectric effect has been studied comprehensively, new features of its manifestation have been reported in recent publications (e.g., passive enhancement of the effect in a pyroelectric film formed on a thick substrate [2, 3] and the nonlinear pyroelectric effect [6]). In the former case, passive amplification of a sinusoidal signal as compared to the situation in a freely suspended sample can be attained in a certain frequency interval. The latter case corresponds to the possibility of using the pyroelectric effect for converting the dissipated thermal energy directly into electric energy [7].

In this study, we analyze the longitudinal and transverse pyroelectric effects in the CS-1029 chiral ferroelectric liquid crystal. In the transverse geometry or in the geometry of freely suspended films, the pyroelectric effect has hardly been investigated at all [8]. An important motivation for studying the pyroelectric effect in this geometry is that freely suspended films have no contact with solid substrates. It is well known that massive substrates considerably reduce the threshold sensitivity and signal-to-noise ratio of pyroelectric pickups [9]. We will demonstrate here that it is possible in principle to detect a pyroelectric signal in a freely suspended ferroelectric liquid-crystal film, and we will give the comparative characteristics of the pyroelectric effect in the two geometries.

2. EXPERIMENTAL

2.1. Preparation of Samples and Liquid-Crystal Cells

The ferroelectric liquid crystal used in our experiments was a CS-1029 (Chisso corporation) optically active smectic liquid crystal. This liquid-crystal mixture contains chiral molecules in the tilted smectic phase C^*, exhibiting spontaneous polarization perpendicular to the liquid-crystal director (directed along the smectic layer) in accordance with symmetry considerations [10]. The CS-1029 liquid-crystal mixture is characterized by the following sequence of phases: Cr (−18°C) SmC^* (73°C) SmA^* (85°C) N^* (95°C) I^* with a spiral pitch $\rho(25°C) = 2$ μm, angle of inclination $\theta(25°C) = 25°$ of molecules to smectic layers, and spontaneous polarization $P_s(25°C) = -41.6$ nC/cm^2. The minus sign of the spontaneous polarization corresponds to the adopted convection [11]. In this case, normal $\mathbf{h}_z$ to the smectic plane, director $\mathbf{n}$ of the liquid crystal, and spontaneous polarization $\mathbf{P}$ form a left triple of vectors. Permittivity $\varepsilon_{\parallel} = 2.9$ and $\varepsilon_{\perp} = 22.2$ at a frequency of 1 kHz and a temperature of 40°C were measured in [12] using commercial (EHC) cells. To intensify bulk absorption of radiation, a small amount of D55* azo dye with the chemical formula shown in Fig. 1 was added to the liquid crystal. The D55* azo dye is a monotropic chiral nematic liquid crystal with the following sequence of phases: Cr (105°C) I^* (104°C) N^* (64°C) Cr. The data were obtained from observation of textures in a polarization microscope and using differential scanning calorimetry. It should be noted that the temperature of the transition to the monotropic nematic phase for D55* had no fixed value and depended on the previous history and rate of cooling of the sample. The optical activity of D55* dye was found to be low. For example, we failed to induce a characteristic cholesteric structure in the 5CB nematic liquid crystal even when high concentrations of the chiral impurity ($c = 3.1\%$, $d = 10$ μm) were used [13]. One of the features of this type of compounds is the possibility of their existence in two isomeric states (trans and cis). Trans-isomers are more stable. The absorption spectrum of precisely this geometrical isomer is shown in Fig. 2. In our experiment, we used two different geometries (longitudinal and transverse). In the longitudinal geometry, commercial sandwich cells (EHCs) 10 μm in thickness

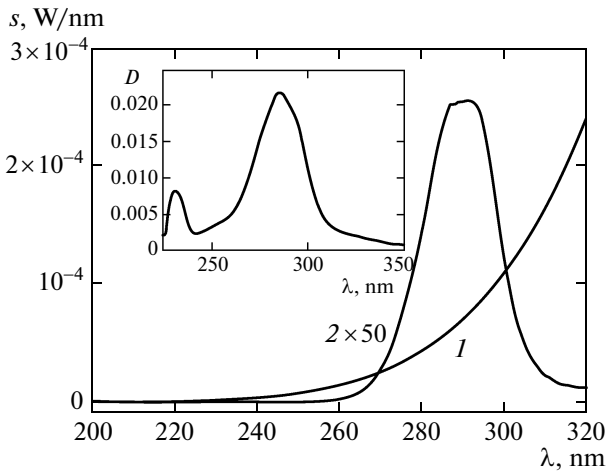

Fig. 2. Spectral density s of radiation power from a tungsten lamp ($T = 2700$°C, $P = 100$ W) (curve *1*) and spectral density of the radiation power absorbed in a freely suspended film containing 1% (by weight) of D55* dye (curve *2*). The inset shows optical density D of the freely suspended CS-1029 + 1%D55* film.

were used as a liquid-crystal cell. The inner surfaces of the cells were treated with polyimide, inducing the planar orientation of the liquid crystal. The CS-1029 liquid crystal in the isotropic phase was pulled into the cell by capillary forces. Then the liquid crystal was cooled to the ferroelectric phase and transformed into a single-domain crystal by alternating high-frequency electric field. When the pyroelectric effect was studied in the transverse geometry, freely suspended liquid-crystal films were used. The films were obtained by "smearing" a small portion of the ferroelectric liquid crystal with a pallet over a slotlike aperture (1 × 10 mm). To increase bulk absorption, D55* dye (1%) was added. The edges of the rectangular slotlike aperture simultaneously served as electrodes. An electric field was applied to the electrodes (blades of razors). The pyroelectric current or voltage was removed from the same electrodes.

2.2. AC Pyroelectric Measurements

Figure 3 shows a block diagram of the setup for studying the pyroelectric effect. The pyroelectric constant was measured using the Czochralski dynamic method [14]. The cells were placed into the thermostabilized chamber (±1°C). The temperature was measured by a copper–constantan thermocouple to within 1°C. In the modulation technique used here, a semiconductor laser ($\lambda = 850$ nm, $P = 40$ mW) was used for periodic heating of the pyroelectric material. The laser modulation frequency f varied from 0.001 Hz to 250 kHz. The pyroelectric effect in the freely suspended film was investigated using a tungsten incandescent lamp ($P = 100$ W); approximately 2% of the electric power corresponded to the visible range. Laser radiation was modulated using the transistor–transistor logic (TTL) microchip. Radiation from the incandescent lamp focused by a lens was modulated by a mechanical chopper as shown in Fig. 4.

The maximum modulation frequency of the chopper did not exceed 500 Hz. The power of transmitted and reflected radiation was measured by FD-7K silicon photodetectors with a large aperture. In our experiment, modulated radiation heated the ferroelectric liquid crystal either due to heat transfer from the ITO electrode absorbing radiation (in the EHC dell) or as a result of bulk absorption by the dye dissolved in the smectic liquid crystal (freely suspended film). Pyroelectric voltage U_p proportional to the pyroelectric constant was removed from the load resistors with $R_{load} = 1$ and 10 MΩ. In this case, we used the EG&G7260 synchronous detector in the voltage-measuring regime. The pyroelectric current i_p was measured directly in the current-measuring regime, but in a much narrower frequency range 0.001 Hz–50 kHz (3 dB at 50 kHz):

$$i_p = \frac{U_p}{R_e} = \frac{dP_s}{dt} = \gamma\frac{dT}{dt}, \qquad (1)$$

where $\gamma = dP_s/dt$ is the pyroelectric constant, $R_e = R_{load}R_i/(R_{load} + R_i)$, R_i is the input resistance of the synchronous amplifier, R_{load} is the load resistance, U_p is the pyroelectric voltage, and T is the temperature. An important factor in the modulation method is independence of the heating rate of temperature, which is observed to a high degree of accuracy as a rule.

The absorption spectrum was measured by an HP-8452A spectrophotometer based on a silicon photodiode matrix consisting of 512 photodetectors.

3. EXPERIMENT AND DISCUSSION OF RESULTS

3.1. EHC Cell

Figure 5 schematically shows the equilibrium orientations of the **c** director under the action of a dc electric field $\mathbf{E}_{BL}$ and $\mathbf{E}_{ITO}$ ($\mathbf{c} \perp \mathbf{E}_{BL}$ and $\mathbf{c} \perp \mathbf{E}_{ITO}$) as in a freely suspended film and EHC cell. The direction of the field for the EHC cell is shown by the dashed arrow.

In the experiment with the EHC cell with CS-1029, constant bias voltage $U_b = 5$ V was applied simultaneously with periodic heating. In this way, we obtained the temperature dependence of pyroelectric constant γ and spontaneous polarization P_s (Fig. 6). The spontaneous polarization was calculated by integrating the pyroelectric constant with respect to temperature. The pyroelectric constant was calibrated by equating the area under the $\gamma(T)$ curve to the spontaneous polarization measured at a fixed temperature. Spontaneous polarization P_s was determined by measuring the switching current using two alternative methods of applying external

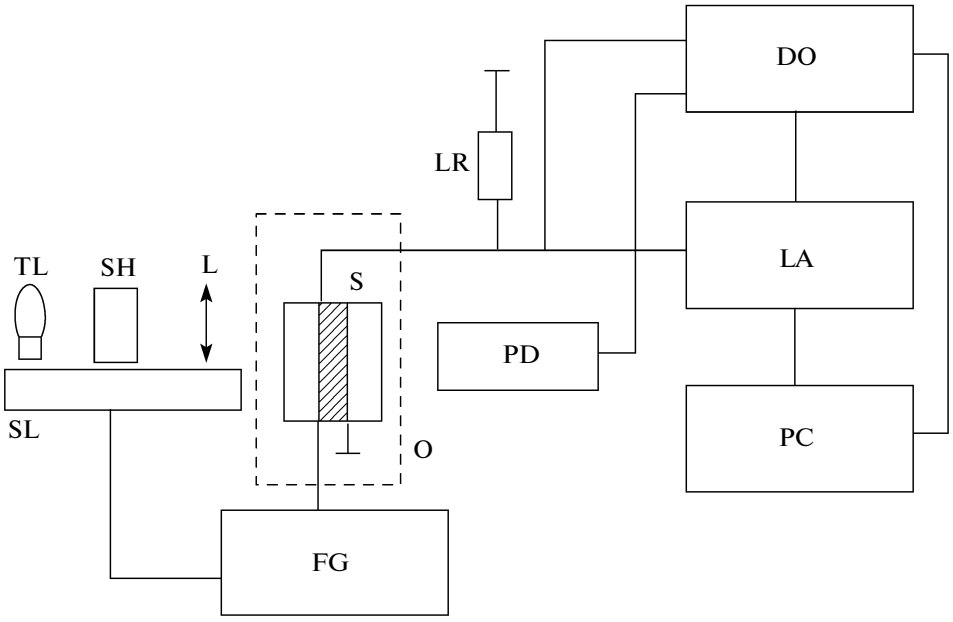

Fig. 3. Block diagram of the experimental setup for studying the pyroelectric effect: TL—incandescent lamp; SH—shutter; SL—semiconductor laser; S—commercial liquid-crystal cell with CS-1029 or freely suspended film; O—heater with a thermostabilizer; FG—ac generator (with possible application of constant bias voltage); PH—photomultiplier; LR—load; DO—digital oscilloscope; LA—E&G7260 synchronous detector; PC—computer.

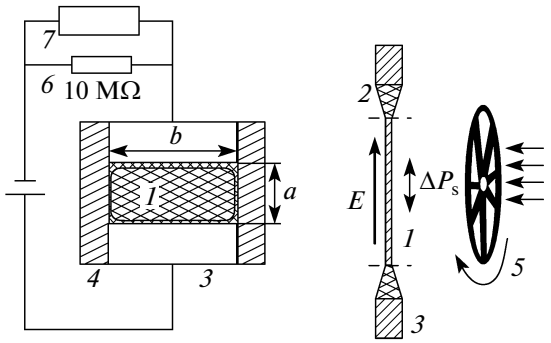

Fig. 4. Setup for analyzing the transverse pyroelectric effect in geometry of freely suspended films: (*1*) CS-1029 + 1%D55*; (*2*) meniscus of a freely suspended film; (*3*) metal electrodes (razor blades); (*4*) movable mylar barriers; (*5*) shutter; (*6*) load resistor of 10 MΩ; (*7*) synchronous detector; E is the static electric field; ΔP_s is the increment of spontaneous polarization upon a change in temperature by ΔT; $a = 1$ mm, $b = 10$ mm.

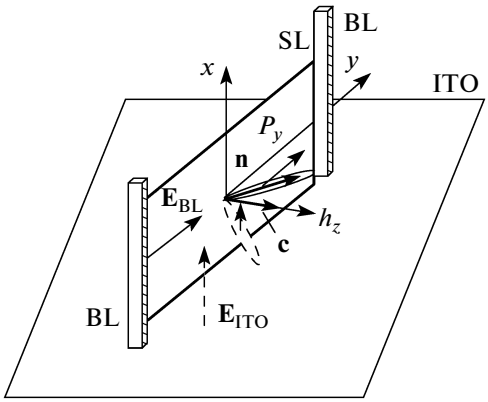

Fig. 5. Diagram explaining the orientation of the **c** director in a freely suspended film in electric field E_{BL} in the gap between two planar electrodes (razor blades). In the EHC cell, the director is oriented by field R_{ITO} (dashed arrow); $\mathbf{h}_z$ is the direction of the spiral axis; BL are planar electrodes (razor blades), ITO are electrodes of the EHC cell.

electric field E in the form of bipolar pulses: (i) of rectangular shape (Merz technique) or (ii) triangular shape technique [15, 16].

In the case of a second-order transition from SmA to SmC* at point $T = 73$°C, spontaneous polarization was zero, while $P_s(25°C) = -41.5$ nC/cm^2. The temperature of the SmA–SmC* transition was obtained from an analysis of the pyroelectric response. The gauge factor k that can be used for obtaining numerical values of the pyroelectric constant for CS-1029 is given in this case by

$$k = P_s\big|_{T = 25°C} \Big/ \int_{25°C}^{73°C} i_p dT. \qquad (2)$$

where i_p is the experimentally measured pyroelectric current as a function of temperature. In a more rigorous analysis, we must also take into account the temperature dependences of c_p and ρ, where c_p and ρ are

the specific heat at constant pressure and the density of the liquid crystal, respectively. In some cases, a correction for the bolometric and flexoelectric effects is introduced [14, 17]. It should be noted that the temperature dependences of c_p, ρ, and ε can be significant, but only in the immediate vicinity of the phase transition. According to [17], the flexoelectric contribution becomes noticeable only for small spiral pitches ($h < 1$ μm) and can be disregarded in our case.

It is worth noting that the maximal value of the pyroelectric constant of CS-1029 (approximately 6 nC/(cm^2 K)) was comparable with that for familiar organic pyroelectrics such as tetra-aminodiphenyl, PVDF, and PVDF-TFE copolymer [18]. Figure 7 shows the frequency dependence of the pyroelectric voltage across the EHC cell. The inset to this figure shows the frequency dependence of the modulus of the pyroelectric signal from CS-1029 in the EHC cell, normalized to its maximal value (curve *1*). The pyroelectric voltage in this case was measured across the load resistor $R_{load} = 1$ MΩ, $R_{load} > R_{in}$, where R_{in} is the input resistance of the synchronous detector. An analogous dependence for the well-known organic pyroelectric guanidine nitrate [19] is shown for comparison (curve *2*). In the case of guanidine, the modulus of the pyroelectric current was measured; i.e., the synchronous detector was used in the current-measuring regime. Curve *3* reproduces the characteristic of the low-frequency filter of the EG&G7260 synchronous detector. The low-frequency branches of curves *1* and *2* describing the pyroelectric response have the universal form $f^{1/2}$ following from the solution to the heat-conduction equation with the corresponding boundary conditions [19, 20]. The pyroelectric current in the high-frequency range is independent of frequency [2–4, 20], which is confirmed by the plateau on curve *2*. The plateau on curve *1* is not exhibited due to the large time constant of the electric circuit: $R_{load} = 1$ MΩ, $C =$ 0.3 nF, and $\gamma = 0.3$ ms. The high-frequency descent on all three curves is determined by the input circuits of the measuring electronic devices.

In the classical work by Chynoweth [14], the equivalence of hysteretic curves $\gamma(E)$ and $P_s(E)$ is demonstrated for barium titanate as an example. Both descriptions are also equivalent for a ferroelectric liquid crystal under certain conditions [21]. For a ferroelectric freely suspended film, we have

$$P_s = \frac{N}{V}\mu\langle\cos\varphi\rangle, \quad (3)$$

$$\gamma = \frac{N}{V}\frac{d\mu}{dT}\langle\cos\varphi\rangle, \quad (4)$$

where N is the number of molecules in the crystal, V is the crystal volume, φ is the azimuthal angle of orientation of the **c** director, and μ is the average dipole moment per molecule (μ ~ θ, where θ is the zenithal angle of the director). It follows hence that the ratio of spontaneous polarization to the pyroelectric constant

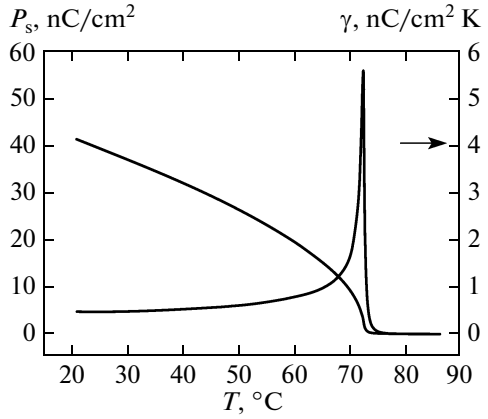

Fig. 6. Pyroelectric constant γ and spontaneous polarization P_s of the CS-1029 ferroelectric liquid crystal as a function of temperature. Bias voltage $U_b = 5$ V. The modulation frequency of the semiconductor laser producing the temperature gradient in the liquid crystal is $f = 1320$ Hz. The rate of temperature variation in the heater is 1°C/s.

at a given temperature is constant. In this case, we can disregard the derivative $d\langle\cos\varphi\rangle/dT$ in view of the weak temperature dependence of the elastic constants, binding energy with the substrate, and dielectric constants far from the phase-transition temperature. It cannot be ruled out that this derivative can be appreciable at the film periphery in the vicinity of the meniscus occupying a much smaller area than the area of a uniformly oriented region of the film. It is precisely due to the geometrical smallness of the transition region of the film that we can disregard its effect on the pyroelectric current being measured. In this case, the temperature dependence of spontaneous polarization is determined by zenith angle θ(T) alone. In this approximation, the hysteresis loop is $\gamma(E)$ ($E \sim U_b$). Figure 8 describes the $P_s(E)$ dependence for CS-1029 both qualitatively and quantitatively. The table gives the characteristic point of hysteresis curve $P_s(U_b)$, viz., E_{sat}, E_c, P_r, and densities of energy s released upon path-tracing of the hysteresis loop.

3.2. Freely Suspended Film

The transverse pyroelectric effect in a freely suspended CS-1029 film with the D55* dye was studied on the setup depicted in Fig. 4. Freely suspended films were formed in the SmA phase ($T = 80$°C) followed by cooling to room temperature. The films were prepared using the minimum amount of LC to reduce the effect of the meniscus on the pyroelectric signal being measured. The homogeneity of the film was monitored visually. The film thickness $d \approx$ 0.2 μm was determined by the Sirota method [22] (i.e., from interference colors). To form the single-domain structure, a constant electric field of about 5×10^2 V/cm, which oriented spontaneous polarization in the field direction, was applied to the ferro-

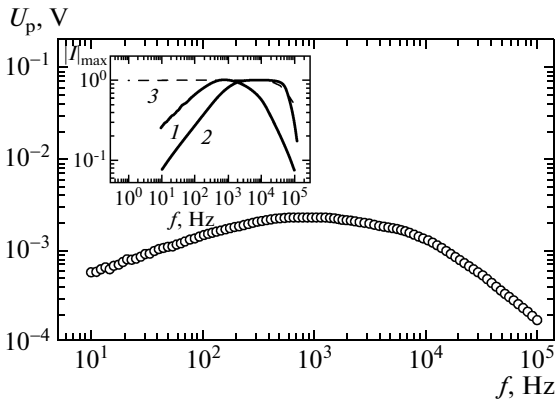

Fig. 7. Pyroelectric voltage U_p as a function of frequency of CS-1029 in the EHC cell. The inset shows the modulus of the pyroelectric signal normalized to its maximal value as a function of frequency for CS-1029 in the EHC cell (d = 10 μm, U_b = 9 V, T = 25°C) (curve *1*) and for guanidine nitrate (curve *2*). Curve *3* describes the transmission for the low-frequency filter of synchronous detector EG&G7260 (3 dB for 50 kHz).

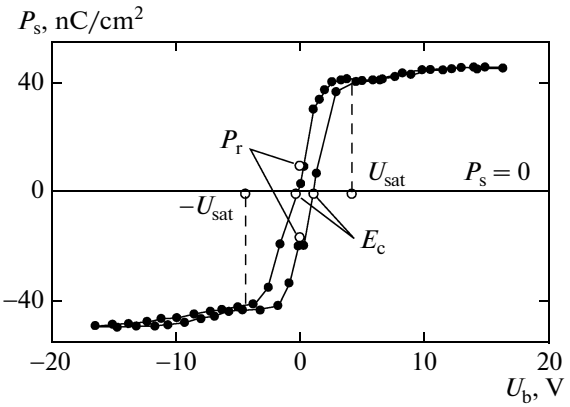

Fig. 8. Ferroelectric hysteresis loop for CS-1029 in the EHC cell in the U_b vs. P_s coordinates; T = 25°C, d = 10 μm, f = 6030 Hz.

electric LC. The reference voltage was tuned to the light beam interruption frequency. The pyroelectric voltage or pyroelectric current was measured by the synchronous detector on the first harmonic of the reference signal. An admissible signal-to-noise ratio was attained for an integration constant of $\tau \approx$ 10 min. The film was illuminated by the periodically interrupted luminous flux from the incandescent lamp with the light beam direction perpendicular to the electric field. The sample was thoroughly screened from stray electric currents. The pyroelectric voltage was measured on a resistance of R_{load} = 10 MΩ. Figure 2 shows spectral density of radiation from a Planck source (tungsten lamp) and the spectral density of the absorbed radiation power calculated taking into account the absorption spectrum of the film. As a result, we calculated the radiation power absorbed by the film taking into account the lens aperture and the diameter of the light spot focused on the film. In these conditions, the absorbed radiation power was P = 2 μW (or 200 μW if we disregard the corrections for the lens aperture and the area of the film).

Figure 9 shows the typical temperature dependences of the pyroelectric voltage for two fixed frequencies of light beam interruption. It should be noted that the singularity of the pyroelectric response near the phase-transition point was accompanied by electrohydrodynamic instability in the film, which deteriorated the signal-to-noise ratio.

Figure 10 shows the dependence of P_s on the applied voltage. It turns out that in the absence of the effect of confining surfaces, the shape of the hysteretic curve is close to that for an ideal "helielectric" [23]. The finite values of the area bounded by the hysteresis loop and of the coercive force were apparently determined by the edge effect (i.e., the influence of the meniscus of the film bordering with solid surfaces). The pyroelectric current at the peak of the signal was 0.42 pA at a frequency of 100 Hz. With allowance for the absorbed power, the ampere–watt sensitivity of the film is 0.2 μA/W. It should be noted that the current sensitivity typical of organic pyroelectric normally does not exceed 1 μA/W [19]. For comparison, the table gives the values of the characteristic points of the hysteresis loop. These data lead to the following relations:

$$\frac{E_c^{EHC}}{E_c^{film}} = 20, \quad \frac{E_{sat}^{EHC}}{E_{sat}^{film}} = 10,$$
$$\frac{P_r^{EHC}}{P_r^{film}} = 2.5\text{–}4, \quad \frac{S^{EHC}}{S^{film}} = 40. \qquad (5)$$

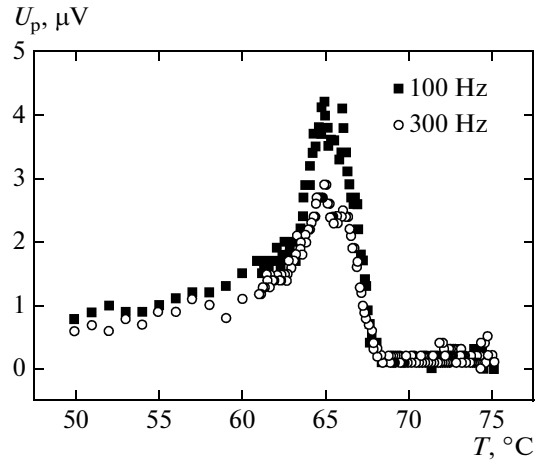

Fig. 9. Pyroelectric voltage U_p in the transverse pyroelectric effect as a function of temperature at two frequencies f_1 = 100 Hz and f_2 = 300 Hz for the CS-1029 + 1%D55* mixture. The temperature of the SmC^*–SmA transition for this mixture is 67.5°C.

Hysteresis in the EHC cell and in a freely suspended film

	E_{sat}, V/μm	E_c, V/μm	P_r, nC/cm^2	s, μJ/cm^3
EHC cell	0.4	0.1	10.4, −19 (25°C, 6030 Hz)	160
Freely suspended CS-1029 film	4×10^{-2}	4.2×10^{-3}	4 (66°C, 300 Hz)	4

E_{sat} is the saturation electric field, E_c is the coercive field, P_r is the residual polarization, and s is the energy density dissipated during path-tracing of the hysteresis loop.

Thus, although the residual polarization for the transverse pyroelectric effect is considerably smaller than for the longitudinal effect, the energy gain after path-tracing of the hysteresis loop is significant (by 40 times); this can be interesting for the application of ferroelectric films in nonvolatile storage devices.

4. CONCLUSIONS

It has been shown experimentally that switching of spontaneous polarization in a chiral ferroelectric liquid crystal, which is detected in the transverse geometry using the pyroelectric effect, occurs under milder conditions than in the longitudinal geometry. Since a polarization state does not decay during information read-out with the help of the pyroelectric effect, and a record small amount of energy is required to change the direction of polarization, the effect of bistability in a ferroelectric liquid crystal in the transverse geometry can find application in nonvolatile storage devices [23].

It should also be noted that in the well-known Clark–Lagerwall effect, the physical reason for bistability in ferroelectric liquid crystals is the change in orientation of the director on the bounding surfaces [24]. It is due to the reorientation of the director on the surface of the polymer film coating the electrodes that specific energy losses appear upon path-tracing of the hysteresis loop. In the case of a high binding energy, the hysteresis loop in the E vs. γ (or E vs. P_s) coordinates degenerates into a line. Analogous behavior was observed in [25] in an analysis of the pyroelectric effect in the polar phase (SmC^*_β) of classical antiferroelectric MHPOBC liquid crystal (4-(1-methylheptyl-oxycarbonylphenyl)4'-actylbuphenyl-4-carboxylate).

An alternative mechanism explaining the experimental results can also be associated with switching of bulk polar (probably, metastable) configurations of the **c** director. The question about the existence of bistability in freely suspended films in the case of an infinitely high binding energy remains unanswered. On the other hand, bistable optical effects were observed in chiral nematic liquid crystals in the case of a high binding energy with the substrate as well. For example, the conditions in which the lifetime of switchable states is sufficient for observation of the bistability effect in real time were formulated in [26, 27].

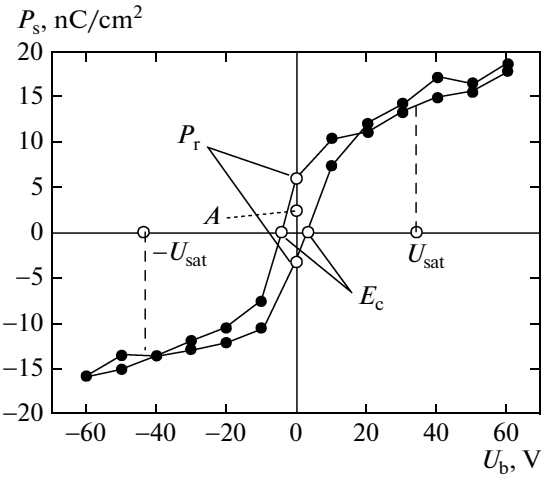

Fig. 10. Ferroelectric hysteresis loop in the transverse pyroelectric effect for a freely suspended film for the CS-1029 + 1%D55* mixture, $T = 66$°C. Point A denotes the beginning of path-tracing for a freshly prepared sample.

ACKNOWLEDGMENTS

This work was supported financially by the Russian Science Foundation (project no. 14-12-00475); Soto-Bustamante and Romero-Hasler express their sincere gratitude to Fondecyt 1130187. The authors also thank M. Kozlovskii for synthesis of the D55* azo dye.

REFERENCES

1. Sidney B. Lang, Phys. Today **58** (8), 31 (2008).
2. S. V. Yablonskii and E. A. Soto-Bustamante, J. Exp. Theor. Phys. **111** (5), 814 (2010).
3. S. V. Yablonskii and E. A. Soto-Bustamante, Mol. Cryst. Liq. Cryst. **541**, 44/[282] (2011).
4. L. S. Kremenchugskii and O. V. Roitsina, *Pyroelectric Radiation Detectors* (Naukova Dumka, Kiev, 1979) [in Russian].
5. V. A. Borisenok, E. Z. Novitskii, and V. G. Simakov, Instrum. Exp. Tech. **52** (4), 523 (2009).
6. B. A. Strukov, Soros. Obraz. Zh. **12**, 94 (1998).
7. Jin Fang, H. Frederich, and L. Pilon, J. Heat Transfer **132**, 092701-1 (2010).

8. S. Yablonskii, T. Oue, H. Nambu, M. Ozaki, and K. Yoshino, in *Proceedings European Conf. on Liquid Crystals (ECLC 1999), Hersonissos, Crete, Greece, April 25–30, 1999* (Hersonissos, 1999), p. 2.
9. P. A. Bogomolov, V. I. Sidorov, and I. F. Usol'tsev, *Detectors for IR-Systems* (Radio i Svyaz', Moscow, 1987), p. 147 [in Russian].
10. R. B. Meyer, L. Liebert, L. Strzelecki, and P. Keller, J. Phys. **36**, L-69 (1975).
11. HandBook of Liquid Crystals, Ed. by D. Demus, J. W. Goodby, G. W. Gray, and H.-W. Spiess, *High Molecular Weight Liquid Crystals* (Wiley, Weinheim, Germany, 1998).
12. S. Lee, K. Nakayama, T. Matsui, M. Ozaki, and K. Yoshino, IEEE Trans. Dielectr. Electr. Insul. **9**, 31 (2002).
13. L. Blinov, M. Kozlovskii, T. Nagate, M. Ozaki, and K. Yoshino, Jpn. J. Appl. Phys. **38**, L1042 (1999).
14. A. G. Chynoweth, J. Appl. Phys. **27**, 78 (1956).
15. W. J. Merz, J. Appl. Phys. **27**, 938 (1956).
16. S. G. Yudin, L. M. Blinov, N. N. Petukhova, and S. P. Palto, JETP Lett. **70** (9), 633 (1999).
17. L. A. Beresnev, V. A. Baikalov, and L. M. Blinov, Ferroelectrics **58**, 245 (1984).
18. E. F. Pevtsov, A. S. Sigov, M. I. Maleto, and A. P. Svotina, in *Proceedings of 14th International Symposium "Thin Films in Optics and Electronics," Kharkov Scientific Assembly (ISTFE-14), National Science Center Kharkov Institute of Physics and Technology, Kharkov, Ukraine, May 22–27, 2002* (Kharkov, 2002), p. 166.
19. S. Yablonskii, E. A. Soto-Bustamante, V. H. Trujillo-Rojo, and V. Sorokin, J. Appl. Phys. **104**, 114102 (2008).
20. A. van der Ziel, J. Appl. Phys. **44**, 546 (1973).
21. S. V. Yablonskii, E. A. Soto-Bustamante, R. O. Vergara-Toloza, and W. Haase, Adv. Mater. (Weinheim) **16**, 1936 (2004).
22. E. B. Sirota, P. S. Pershan, L. B. Sorensen, and J. Collet, Phys. Rev. E: Stat. Phys., Plasmas, Fluids, Relat. Interdiscip. Top. **36**, 2890 (1987).
23. K. Bourzac, Nat. News (June 11, 2013). doi 10.1038/nature.2013.13169
24. S. T. Lagerwall, J. Phys. Condens. Matter **8**, 9143 (1996).
25. S. V. Yablonskii, K. Nakano, M. Ozaki, and K. Yoshino, J. Exp. Theor. Phys. **100** (2), 422 (2005).
26. D. W. Berreman and W. R. Heffner, Appl. Phys. Lett. **37**, 109 (1980).
27. S. P. Palto and M. I. Barnik, J. Exp. Theor. Phys. **100** (1), 199 (2005).

Translated by N. Wadhwa